Eur. Phys. J. A **8**, 537–548 (2000)

THE EUROPEAN PHYSICAL JOURNAL A

Inclusive meson production in peripheral collisions of ultrarelativistic heavy ions

K.A. Chikin[1,a], V.L. Korotkih[1,b], A.P. Kryukov[1,c], L.I. Sarycheva[1,d], I.A. Pshenichnov[2,e], J.P. Bondorf[3,f], and I.N. Mishustin[3,4,g]

[1] Institute of Nuclear Physics, Moscow State University, 119899 Moscow, Russia
[2] Institute for Nuclear Research, Russian Academy of Science, 117312 Moscow, Russia
[3] Niels Bohr Institute, DK-2100 Copenhagen, Denmark
[4] Kurchatov Institute, Russian Research Center, 123182 Moscow, Russia

Received: 23 February 2000 / Revised version: 5 July 2000
Communicated by W. Henning

Abstract. There exist several proposals to use Weizsäcker-Williams photons generated by ultrarelativistic heavy ions to produce exotic particles in $\gamma\gamma$ fusion reactions. To estimate the background conditions for such reactions we analyze various mechanisms of meson production in very peripheral collisions of ultrarelativistic heavy ions at RHIC and LHC energies. Besides the $\gamma\gamma$ fusion they include also electromagnetic γA interactions and strong nucleon-nucleon interactions in grazing AA collisions. All these processes are characterised by low multiplicities of produced particles. The γA and AA events are simulated by corresponding Monte Carlo codes, RELDIS and FRITIOF. In each of these processes a certain fraction of pions is produced close to the mid-rapidity region that gives a background for the $\gamma\gamma$ events. The possibility of selecting the mesons produced in the $\gamma\gamma$ fusion events via different p_t cut procedures is demonstrated.

PACS. 25.75.-q Relativistic heavy-ion collisions – 25.75.Dw Particle and resonance production

1 Introduction

According to the impact parameter b, different phenomena take place in collisions of ultrarelativistic heavy ions. They can be divided into the following three categories.

Central collisions ($b \approx 0$), *i.e.* the collisions with nearly full nuclear overlap fall into the first category. Such collisions provide conditions for the creation of very hot and dense nuclear matter. It is the aim of future experimental programs at the Large Hadron Collider (LHC) at CERN [1] and the Relativistic Heavy Ion Collider (RHIC) at Brookhaven National Laboratory [2] to study a possible phase transition of the nuclear and hadronic matter into the so-called quark-gluon plasma at high energy densities. Such extreme conditions are believed to be similar to those existed in the Early Universe soon after the Big Bang.

The second category contains collisions with partial overlap of nuclei ($b < R_1 + R_2$, R_1 and R_2 are the nuclear radii). In such collisions the residual spectators remain relatively cold. Short-range interaction via the strong nuclear forces is restricted mainly to the participant zone. In the whole set of minimum-bias events the number of peripheral nuclear collisions is significant due to the geometrical factor $2\pi b$. The general picture of ultrarelativistic heavy-ion collisions at LHC and RHIC will be incomplete without considering such peripheral collisions. Noncentral heavy-ion collisions are considered as a place to look for the disoriented chiral condensates [3] and elliptic flow [4]. Combining the Hanbury-Brown-Twiss method with the determination of the reaction plane [5] one is able to study the size, deformation and opacities of the particle emission sources. With the aim to study central collisions, one has to know the exact properties of the complementary peripheral collisions. A proper rejection of these "background" collision events will be crucial for extracting the events in which the quark-gluon plasma may be created.

In the collisions of the third category the impact parameter exceeds the sum of nuclear radii ($b > R_1 + R_2$). Therefore, there is no overlap of nuclear densities, but nevertheless, one or both nuclei may be disintegrated by the long-range electromagnetic forces. This process of the Electromagnetic Dissociation (ED) is a well-known phenomenon [6–8]. The interaction can be treated in terms

[a] e-mail: const@lav1.npi.msu.su
[b] e-mail: vlk@lav1.npi.msu.su
[c] e-mail: kryukov@theory.npi.msu.su
[d] e-mail: lis@alex.npi.msu.su
[e] e-mail: pshenichnov@nbi.dk
[f] e-mail: bondorf@nbi.dk
[g] e-mail: mishustin@nbi.dk

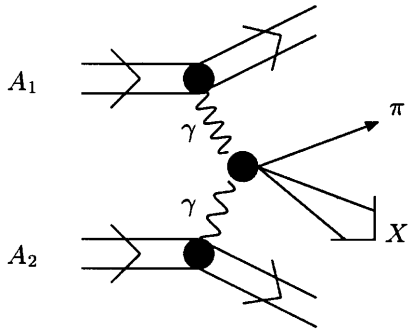

Fig. 1. Meson production in $\gamma\gamma$ fusion.

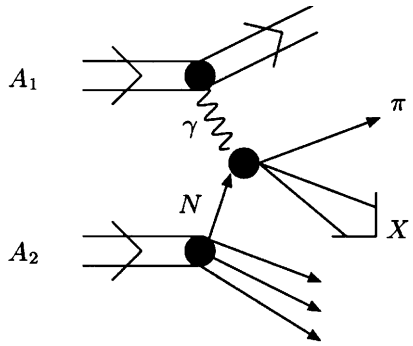

Fig. 2. Meson production in γA collision.

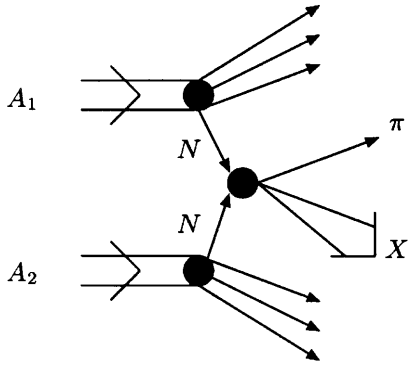

Fig. 3. Meson production in grazing AA collision.

of equivalent photons representing the Lorentz-boosted Coulomb field of heavy ions. At ultrarelativistic energies the ED cross-section exceeds considerably the pure nuclear cross-section for heavy colliding nuclei. This fact was confirmed recently in experiments [9]. The electromagnetic collision events are less violent than the collisions with nuclear interactions. Thus the average particle multiplicities are essentially lower [10,11] and the main part of nucleons and mesons is produced in the regions of projectile and target fragmentation, very far from the mid-rapidity region.

Besides the action of virtual (equivalent) photons on colliding nuclei, the photons from two nuclei can collide (fuse) and produce various secondary particles. Photon-photon ($\gamma\gamma$) physics may be investigated in such collisions [7,8,12]. The idea to produce exotic particles via the $\gamma\gamma$ fusion in heavy-ion colliders has been put forward more than 10 years ago in ref. [13]. Many authors have further developed this idea since that time. The production of different particles from $\mu^{\pm}$, $\tau^{\pm}$ leptons to Higgs bosons and supersymmetric particles has been considered. The full list of references can be found in the recent reviews [7,8].

As one can see, there exist several mechanisms of the particle production in peripheral collisions of ultrarelativistic heavy ions: the $\gamma\gamma$ fusion, γA interaction and grazing nuclear collisions (see figs. 1–3). In the present paper we study the production of $\pi^{\pm}$ and π^0 mesons via these mechanisms. We discuss the general features of the pion production and calculate the contributions of different mechanisms. Prior to investigating exotic-particle production in $\gamma\gamma$ collisions a certain "calibration" is necessary for the theoretical methods and experimental techniques.

Similar investigations have been performed specially for the STAR detector at RHIC [14,15] and the corresponding acceptance cuts were applied from the beginning. The CMS detector which will be installed at LHC [16] can also be used for studying the meson production in peripheral collisions. Even having in mind a plan to use another experimental set-up for such studies one can estimate first the $\gamma\gamma$ signal-to-background ratio without any acceptance cuts. Such comparison of different mechanisms provides a guide-line which is free of limitations and restrictions of existing experimental facilities. This is useful for possible extensions and updates of the existing detectors.

In the present paper we pay the main attention to the inclusive cross-sections of the meson production by different mechanisms. This study is complementary to a very recent one [17], which deals with the exclusive meson production channels. As we expect, in order to select the rare events with a single vector meson [17], one has to reject the background due to the meson production (π^+, π^-, π^0) via the γA process. This background may be estimated in the framework of the models used in the present paper.

A meson production event may be followed by a partial disintegration of a nucleus. We study such reactions in addition to the coherent meson production process considered in ref. [17] when the colliding nuclei remain intact. Different characteristics of the pion production by equivalent photons are calculated by the RELDIS code [11] based on the extended model of photonuclear reactions [18]. The FRITIOF Monte Carlo event generator, version 7.1 [19] is used to study the properties of grazing nuclear collisions.

2 Distant electromagnetic collisions

2.1 Equivalent photon spectra

Let us consider a point-like charge Ze moving with velocity v at impact parameter b. In the Weizsäcker-Williams approximation [6–8] the spectrum of equivalent photons is given by

$$N(\omega, b) = \frac{Z^2\alpha}{\pi^2 b^2 \beta^2} x^2 \left(K_1^2(x) + \frac{1}{\gamma^2} K_0^2(x) \right) , \qquad (1)$$

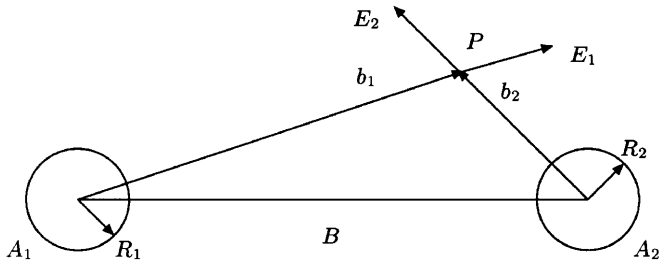

Fig. 4. Effective $\gamma\gamma$ luminosity for heavy-ion collisions. The beam direction is perpendicular to the picture plane. b_1 and b_2 are the distances from the nuclear centers to the photon interaction point P.

where $x = \omega b/\gamma v$, $\beta = v/c$ and $\gamma = (1-\beta^2)^{-1/2}$ is the Lorentz factor of the moving charge. K_0 and K_1 are the modified Bessel functions of zero and first order.

The total number of photons with the energies ω_1 and ω_2 colliding at the point P is obtained by the integration of the equivalent photon spectra over the distances b_1 and b_2 [20] (see fig. 4):

$$F(\omega_1,\omega_2) = 2\pi \int_{R_1}^{\infty} b_1 \mathrm{d}b_1 \int_{R_2}^{\infty} b_2 \mathrm{d}b_2 \times \int_0^{2\pi} \mathrm{d}\phi N(\omega_1,b_1) N(\omega_2,b_2) \Theta(B^2), \quad (2)$$

where R_1 and R_2 are the nuclear radii, Θ is the step function and $B^2 = b_1^2 + b_2^2 - 2b_1 b_2 \cos\phi - (R_1+R_2)^2$.

The $\gamma\gamma$ luminosity calculated in the double equivalent photon approximation [20] is

$$\frac{\mathrm{d}^2 L}{\mathrm{d}W \mathrm{d}y} = \frac{2}{W} F\left(\frac{W}{2}e^y, \frac{W}{2}e^{-y}\right), \quad (3)$$

where the energy squared $W^2 = 4\omega_1\omega_2$ and the rapidity $y = 1/2\ \ln(\omega_1/\omega_2)$ of the $\gamma\gamma$ system were introduced.

The transverse momentum of a produced single meson turns out to be small $p_\mathrm{t} \leq 1/R_{1,2}$ [8,12]. Different nuclear charge form factors may be used in calculations [8,12], but in any approximation the p_t values for the produced meson turns out to be less than 30 MeV/c in PbPb collisions. In the following we shall see how this feature may be used to disentangle $\gamma\gamma$ events from other processes.

2.2 Production of a single meson in $\gamma\gamma$ fusion

The production of a single meson in the $\gamma\gamma$ fusion is the simplest process to analyze. The calculation technique within the framework of the Weizsäcker-Williams formalism for such a process is well known [8,20].

The cross-section to produce a meson with mass M_R is given by

$$\sigma = \int \frac{\mathrm{d}\omega_1}{\omega_1} \int \frac{\mathrm{d}\omega_2}{\omega_2} F(\omega_1,\omega_2) \sigma_{\gamma\gamma\to M_R}, \quad (4)$$

where the number of colliding photons, $F(\omega_1,\omega_2)$, is taken from eq. (2). Taking $\Theta = 1$ one can simplify the calculation, since in this case the integral of eq. (2) may be reduced to the product of the Weizsäcker-Williams spectra, $N(\omega)$, integrated over the impact parameter [6–8]. For light mesons, $M_R \ll \gamma/(R_1+R_2)$, the resulting integral is changed by several percent only. This simplification may be not appropriate for heavy mesons, since they can only be produced by a pair of photons from the high-energy tail of the equivalent photon spectrum. Such mesons are produced mainly in close collisions, where $b \approx R_1 + R_2$ and the region of nuclear overlap cannot be neglected.

The cross-section of the elementary process $\gamma\gamma \to M_R$ may be calculated [7,8,20] as

$$\sigma_{\gamma\gamma\to M_R} = 8\pi^2 (2J_R+1) \Gamma_{M_R\to\gamma\gamma} \delta(W^2 - M_R^2)/M_R, \quad (5)$$

where J_R, M_R and $\Gamma_{M_R\to\gamma\gamma}$ are the spin, mass and two-photon decay width of the meson R. W^2 is the c.m. energy squared of the colliding photons.

The corresponding differential cross-section for producing a meson with mass M_R is given by

$$\frac{\mathrm{d}\sigma_R}{\mathrm{d}y} = 8\pi^2 (2J_R+1) \Gamma_{M_R\to\gamma\gamma} F\left(\frac{M_R}{2}e^y, \frac{M_R}{2}e^{-y}\right)/M_R^3. \quad (6)$$

The exclusive cross-sections for producing a single meson were calculated by many authors. In ref. [7] the equivalent photon cross-section has been derived directly from the first QED principles. Three types of nuclear form factors were used in the calculations [7] corresponding to a homogeneously charged sphere, a Gaussian-shaped and a point-like charge distributions. In this respect the approach of ref. [7] is different from the more phenomenological method of ref. [20] which we basically follow. Moreover, even following the authors of ref. [20] one can use different values for the nuclear radii, $R_{1,2}$. The real nuclear charge distribution with a diffuse boundary should be approximated by a distribution with a sharp boundary that leads to some uncertainties. A straightforward comparison of the results of different authors [7,8,20] seems to be difficult due to different values of M_R, $\Gamma_{\gamma\gamma\to M_R}$ and $R_{1,2}$ used in the different papers.

With the aim to understand the sensitivity of numerical results to the choice of parameters, we repeated the calculations of the cross-section for the single-meson production in ultrarelativistic heavy-ion collisions, see Tables 1–3. We used the same M_R and $\Gamma_{M_R\to\gamma\gamma}$ values as in papers [7,8,20]. All the cross-sections were calculated for the nuclear radii $R_{1,2} = 1.2A^{\frac{1}{3}}$.

As one can see from Tables 1–3, the different approaches give quite similar results for the lightest mesons π^0, η. On the contrary, as it was expected, the difference is noticeable for heavy mesons like η_b, η_c. Nevertheless, this situation seems to be acceptable due to the following reasons. First, in the present paper we will consider mainly the production of the lightest π-mesons. Second, because of uncertainties in the Particle Properties Data on M_R and $\Gamma_{M_R\to\gamma\gamma}$ for heavy mesons [21][1], it is difficult

[1] This is particularly true for the scalar mesons $f_0(975)$ and $f_0(1275)$ with large decay widths causing a strong overlap of individual resonances, see details in ref. [21].

Table 1. Exclusive cross-sections of single-meson production in $\gamma\gamma$ fusion process in ultrarelativistic UU and PbPb collisions at colliders. The values were calculated for comparison with ref. [20]. The masses and two-photon decay widths for pseudoscalar mesons were used according to ref. [20].

			cross-section (mb)			
Meson	M_R	$\Gamma_{M_R\to\gamma\gamma}$	$Z=92$ $A=238$ $\gamma=100$		$Z=82$ $A=208$ $\gamma=4000$	
	(GeV)	(keV)	[20]	this work	[20]	this work
π^0	0.135	0.009	7.9	9.55	49	53.1
η	0.549	1	2.9	3.61	43	45.8
η'	0.958	5	1.1	1.48	30	31.9
η_c	2.981	6.3	$2.5\cdot10^{-3}$	$4\cdot10^{-3}$	0.59	0.644
η_b	9.366	0.41	$7\cdot10^{-9}$	$3.36\cdot10^{-8}$	0.46	$5\cdot10^{-4}$

Table 2. Exclusive cross-sections of single-meson production in $\gamma\gamma$ fusion process in ultrarelativistic PbPb collisions at LHC. The values were calculated for comparison with ref. [8]. The masses and two-photon decay widths for $c\bar{c}$ and $b\bar{b}$ mesons were used according to ref. [8].

			cross-section (mb)	
Meson	M_R	$\Gamma_{M_R\to\gamma\gamma}$	$Z=82$ $A=208$ $\gamma=2750$	
	(GeV)	(keV)	[8]	this work
η'	0.958	4.2	22	20.68
η_c	2.981	7.5	0.59	0.552
χ_{0c}	3.415	3.3	0.16	0.145
η_b	9.366	0.43	$3.7\cdot10^{-4}$	$3.46\cdot10^{-4}$
η_{0b}	9.860	$2.5\cdot10^{-2}$	$1.8\cdot10^{-5}$	$1.62\cdot10^{-5}$
η_{2b}	9.913	$6.7\cdot10^{-3}$	$2.3\cdot10^{-5}$	$2.13\cdot10^{-5}$

Table 3. Exclusive cross-sections of single-meson production in $\gamma\gamma$ fusion process in ultrarelativistic AuAu and PbPb collisions at RHIC and LHC. The values were calculated for comparison with ref. [7]. The masses and two-photon decay widths for different scalar and pseudoscalar mesons were used according to ref. [7].

			cross-section (mb)			
Meson	M_R	$\Gamma_{M_R\to\gamma\gamma}$	$Z=79$ $\gamma=108$		$Z=82$ $\gamma=2750$	
	(GeV)	(keV)	this work	[7]	this work	[7]
π^0	0.135	0.0077	4.744	5.721	37.701	42.937
η	0.547	0.51	1.127	1.285	18.744	19.897
η'	0.958	4.5	0.826	0.989	22.152	24.780
$f_0(975)$	0.974	0.25	0.042	0.0909	1.159	2.496
$f_0(1250)$	1.25	3.4	0.177	0.332	6.360	11.728
f_2	1.275	3.19	0.757	0.679	27.751	24.674
a_2	1.318	1.14	0.230	0.252	8.784	9.542
π_2	1.670	1.41	0.087	0.104	4.547	5.188
f_4	2.05	1.4	0.053	0.0221	3.795	1.605
η_c	2.98	6.3	$3.18\cdot10^{-3}$	$3.66\cdot10^{-3}$	0.464	0.555
χ_{0c}	3.42	5.6	$1.21\cdot10^{-3}$	$1.36\cdot10^{-3}$	0.243	0.290
η_b	9.37	0.4	$3.15\cdot10^{-8}$	$2\cdot10^{-8}$	$3.22\cdot10^{-4}$	$4.06\cdot10^{-4}$

to predict with confidence the exclusive cross-section values for such mesons. Therefore, the uncertainties of the method itself become less important for heavy mesons.

2.3 Inclusive π^0 production within the DRP model

Obviously, the pions can be produced not only in the direct one-step process $\gamma\gamma\to\pi^0$. The $\gamma\gamma$ fusion may lead to the production of several unstable heavy mesons such as η, f_0,... and their decay products may contain π^0's. As one can see in the following, such two-step processes, $\gamma\gamma\to R\to\pi^0$X, with the intermediate meson R give a sizable contribution to the inclusive π^0 production cross-section. In addition to the direct process, reasonable estimation for the inclusive cross-section $\gamma\gamma\to\pi^0$X should contain the sum of dominant contributions from the intermediate meson resonances which contain at least one π^0-meson in the final state. We call this approach a Dominant Resonance Production (DRP) model.

The exclusive differential cross-section, $d\sigma_R/dy$, to produce a single meson R with the mass M_R is given by eq. (6). In the DRP approximation the inclusive cross-section of the π^0 production through the decay of inter-

mediate resonances is

$$\frac{\mathrm{d}\sigma_{\mathrm{incl}}}{\mathrm{d}y}(\pi^0) = \sum_{R,k} \frac{\mathrm{d}\sigma_R}{\mathrm{d}y}\ B_R^{(k)}(R \to \pi^0)\ n_R^{(k)}(\pi^0), \qquad (7)$$

where $B_R^{(k)}(R \to \pi^0)$ is the branching ratio for the decay of the resonance R to the channel k which contains at least one π^0. $n_R^{(k)}(\pi^0)$ is the number of π^0's in the corresponding channel k. If the first step decay products contain another resonance, a similar expression may be written in turn for the second step decays producing π^0. Introducing the value

$$B_R^{\mathrm{out}} = \sum_k\ B_R^{(k)}(R \to \pi^0)\ n_R^{(k)}(\pi^0), \qquad (8)$$

one can rewrite eq. (7) in the following way:

$$\frac{\mathrm{d}\sigma_{\mathrm{incl}}}{\mathrm{d}y}(\pi^0) = \sum_R \frac{\mathrm{d}\sigma_R}{\mathrm{d}y}\ B_R^{\mathrm{out}}. \qquad (9)$$

Particle Data information relevant to the calculation of σ_{incl} is given in Table 4. We selected the resonances with relatively large widths $\Gamma_{M_R\to\gamma\gamma}$. The values of Γ_{tot} and $B_R^{\mathrm{in}} = \Gamma_{M_R\to\gamma\gamma}/\Gamma_{\mathrm{tot}}$ from review [21] which are necessary to calculate $\Gamma_{M_R\to\gamma\gamma}$, are given for completeness. On the contrary to Tables 1–3, the decay probabilities and meson widths in Table 4 were taken according to the most recent version of the Review of Particle Physics [21]. We assumed that the decays $\mathrm{f}_0(980) \to \pi\pi$ and $\mathrm{f}_0(1370) \to \pi\pi$ take place with 100% probability since there is no quantitative information in ref. [21] on other channels. Isospin conservation relations provide the probability of 1/3 for the $\pi^0\pi^0$ charge state in such $\pi\pi$ channels.

The integrated inclusive cross-section of the π^0 production in PbPb collisions ($R_1 = R_2 = 7.75$ fm) at LHC energies is found to be $\sigma_{\mathrm{incl}}(\pi^0) = 106$ mb in the DRP model, while the exclusive one is only 36.3 mb. As one can see, the contribution to the π^0 production via the intermediate resonances turns out to be essential. The corresponding rapidity distributions, $\mathrm{d}\sigma/\mathrm{d}y$, will be discussed in section 4.

2.4 Pion production in γA collisions

The meson production induced by equivalent photons in peripheral collisions of ultrarelativistic heavy ions (fig. 2) is a poorly explored phenomenon. To the best of our knowledge, the first calculations of the total rate of the pion production in electromagnetic collisions were made in ref. [23]. The first experimental evidence of the electromagnetic dissociation accompanied by the pion production was found in ref. [24] for 200 AGeV ^{16}O ions. Due to a small number of the pion production events detected in nuclear emulsion, the absolute cross-section for such dissociation channel was not determined. To date only the existence of the pion production in γA collisions is demonstrated by the experiment [24].

Let us consider the process when an equivalent photon is absorbed by a nucleus leading to the pion production (fig. 2). The nucleus may absorb one or more virtual photons during a collision. We follow Llope and Braun-Munzinger [25] in the description of such multiple absorption processes. The double differential cross-section of the pion production via the single-photon absorption may be written first in the projectile rest frame. In such a frame the nucleus is at rest prior to the absorption:

$$\frac{\mathrm{d}^2\tilde{\sigma}^{(1)}}{p_{\mathrm{t}}\mathrm{d}p_{\mathrm{t}}\mathrm{d}y} = \int\limits_{\omega_{\min}}^{\infty} \frac{\mathrm{d}\omega_1}{\omega_1} N^{(1)}(\omega_1)\sigma_{\mathrm{A}_2}(\omega_1)\frac{\mathrm{d}^2W}{p_{\mathrm{t}}\mathrm{d}p_{\mathrm{t}}\mathrm{d}y}(\omega_1), \quad (10)$$

where σ_{A_2} is the total photoabsorption cross-section for the nucleus A_2 and $\mathrm{d}^2W/p_{\mathrm{t}}\mathrm{d}p_{\mathrm{t}}\mathrm{d}y$ is the double differential distribution of pions produced by the photon with the energy ω_1. A spectral function $N^{(1)}$ is given by the following expression:

$$N^{(1)}(\omega_1) = 2\pi \int\limits_{b_{\min}}^{\infty} b\mathrm{d}b e^{-m(b)} N(\omega_1, b), \qquad (11)$$

where $N(\omega_1, b)$ is defined by eq. (1) and $m(b)$ is the mean number of photons absorbed by the nucleus A_2 in a collision at the impact parameter b:

$$m(b) = \int\limits_{\omega_{\min}}^{\infty} N(\omega, b)\sigma_{\mathrm{A}_2}(\omega)\frac{\mathrm{d}\omega}{\omega}. \qquad (12)$$

Analogously, for the second-order process with a pair of photons absorbed by the nucleus A_2 the double differential cross-section is

$$\frac{\mathrm{d}^2\tilde{\sigma}^{(2)}}{p_{\mathrm{t}}\mathrm{d}p_{\mathrm{t}}\mathrm{d}y} = \int\limits_{\omega_{\min}}^{\infty}\int\limits_{\omega_{\min}}^{\infty} \frac{\mathrm{d}\omega_1}{\omega_1}\frac{\mathrm{d}\omega_2}{\omega_2} N^{(2)}(\omega_1, \omega_2) \times \sigma_{A_2}(\omega_1)\sigma_{\mathrm{A}_2}(\omega_2)\frac{\mathrm{d}^2W(\omega_1)}{p_{\mathrm{t}}\mathrm{d}p_{\mathrm{t}}\mathrm{d}y}\frac{\mathrm{d}^2W(\omega_2)}{p_{\mathrm{t}}\mathrm{d}p_{\mathrm{t}}\mathrm{d}y}, \qquad (13)$$

with the corresponding double-photon spectral function:

$$N^{(2)}(\omega_1, \omega_2) = \pi \int\limits_{b_{\min}}^{\infty} b\mathrm{d}b e^{-m(b)} N(\omega_1, b) N(\omega_2, b). \quad (14)$$

In the above expressions $b_{\min}$ is the minimal value of the impact parameter which corresponds to the onset of nuclear interaction. In pion production calculations the integration over the photon energy starts from $\omega_{\min} \approx 140$ MeV which corresponds to the pion emission threshold. Finally, with the corresponding Lorentz boost from the nucleus rest frame to the laboratory system one can obtain the double differential distribution $\mathrm{d}^2\sigma/p_{\mathrm{t}}\mathrm{d}p_{\mathrm{t}}\mathrm{d}y$ for the produced pions suitable for measurements in experiments. Further details of our approach may be found in refs. [10, 11].

As was shown in ref. [11], the contribution to the pion production from the double-photon absorption is less than 10% for heavy ions with $\gamma \gg 100$. Since the contribution from the third- and fourth-order processes are expected to

Table 4. Resonances, their decay modes and branching ratios (given in brackets) which were taken into account in the inclusive cross-section calculations within the DRP model.

Channel	M_R (GeV)	$\Gamma_{\rm tot}$ (GeV)	$B_R^{\rm in}$	1st decay step	2nd decay step	$B_R^{\rm out}$
$\gamma\gamma \to \pi^0$	0.135	$7.0{\cdot}10^{-9}$	1.	π^0		1
$\gamma\gamma \to \eta$	0.547	$1.18{\cdot}10^{-6}$	0.388	$\eta \to 3\pi^0$ (0.32)		1.19
				$\eta \to \pi^+\pi^-\pi^0$ (0.23)		
$\gamma\gamma \to \eta'$	0.958	$2.03{\cdot}10^{-4}$	0.021	$\eta' \to \pi^0\pi^0\eta$ (0.21)	$\eta \to 3\pi^0$ (0.32)	1.18
					$\eta \to \pi^+\pi^-\pi^0$ (0.23)	
				$\eta' \to \pi^+\pi^-\eta$ (0.44)	$\eta \to 3\pi^0$ (0.32)	
					$\eta \to \pi^+\pi^-\pi^0$ (0.23)	
$\gamma\gamma \to {\rm f}_0$	0.980	0.07	$1.19{\cdot}10^{-5}$	${\rm f}_0 \to \pi^0\pi^0$ (0.33)		0.66
$\gamma\gamma \to {\rm f}_2$	1.275	0.185	$1.32{\cdot}10^{-5}$	${\rm f}_2 \to \pi^0\pi^0$ (0.28)		0.70
				${\rm f}_2 \to \pi^+\pi^-2\pi^0$ (0.07)		
$\gamma\gamma \to {\rm a}_2$	1.318	0.107	$9.4{\cdot}10^{-6}$	${\rm a}_2 \to \eta\pi^0$(0.15)	$\eta \to 3\pi^0$ (0.32)	0.33
					$\eta \to \pi^+\pi^-\pi^0$(0.23)	
$\gamma\gamma \to \pi_2$	1.670	0.258	$5.6 \cdot 10^{-6}$	$\pi_2 \to {\rm f}_2\pi^0$ (0.56)	${\rm f}_2 \to \pi^0\pi^0$ (0.28)	1.10
					${\rm f}_2 \to \pi^+\pi^-2\pi^0$ (0.07)	
				$\pi_2 \to {\rm f}_0(1370)\pi^0$ (0.09)	${\rm f}_0(1370) \to \pi^0\pi^0$(0.33)	

be even lower, these processes can be safely disregarded for the ultrarelativistic energies.

Because of the coherent action of all the charges in the nucleus, the virtuality of the equivalent photon, $Q^2 = -q^2$, is small. Such photons are almost real, $Q^2 \leq 1/R^2$, where R is the nuclear radius. Therefore, photonuclear data obtained in experiments with monoenergetic photons may be used, in principle, as an input for the Weizsäcker-Williams calculations of pion production in γA collisions. Since the spectrum of equivalent photons covers a very wide range of the photon energies, one needs the double differential distribution ${\rm d}^2W(\omega)/p_{\rm t}{\rm d}p_{\rm t}{\rm d}y$ for the photon energies ω starting from the pion emission threshold and up to several tens or even hundreds of GeV.

In the region of interest, *i.e.* at $\omega \geq 140$ MeV, the photon de Broglie wavelength is comparable or even smaller than the nucleon radius. A photon interacts, mainly, with individual intranuclear nucleons. Experimental data on the single-pion photoproduction on the nucleon are accumulated in compilations of refs. [26,27]. The latter compilation contains also the experimental data on photoproduction of baryon, B*, and meson M* resonances: $\gamma{\rm N} \to \pi{\rm B}^\star$ and $\gamma{\rm N} \to \pi{\rm M}^\star$ as well as on some channels of multiple pion production: $\gamma{\rm N} \to i\pi{\rm N}$, $2 \leq i \leq 8$. Due to a long mean free path, an equivalent photon may be absorbed deeply in the nuclear interior. The mesons produced in a photonucleon reaction interact with other intranuclear nucleons inducing different reactions in the nuclear medium. In other words, the process shown in fig. 2 is followed by the final-state interaction of produced hadrons with the residual nucleus A_2. Beside the pions several nucleons may be emitted and the residual nucleus may receive high excitation energy.

Since the data on the pion photoproduction on nuclei exist only for limited domains of ω and pion kinematical variables, a theoretical model should be used in the cases when the data are not available. A suitable tool for describing such multi-step photonuclear reactions is the Intranuclear Cascade Model, which has been well known for many years [28].

As shown in ref. [18], the extended Intranuclear Cascade Model of photonuclear reactions describes reasonably well available data on meson production and nucleon emission obtained in the last two decades with intermediate energy quasi-monochromatic photons. With this in mind one can use the INC model for the Weizsäcker-Williams calculations, as it was demonstrated in refs. [10,11]. Formally, we use 1 TeV as the upper limit for the equivalent photon energy in the γA process. Our model was not initially designed for such high energies when events with a very high hadron multiplicity become possible and many other channels, like baryon-antibaryon photoproduction, may be open. Nonetheless, one can safely use the model to investigate the γA processes with a low multiplicity which represent a background for the $\gamma\gamma$ fusion. Such processes take place mainly at $\omega < 10$ GeV, where our model has been verified in detail.

2.4.1 Simulation of γN interaction

The channels of the hadron photoproduction on the nucleon which are taken into account in the model are listed in Table 5. To describe the two-body photoproduction channels we have basically used the Monte Carlo event generator of Corvisiero *et al.* [29]. The contribution from the two-body channel $\gamma{\rm N} \to \pi{\rm N}$ dominates up to $\omega \approx 0.5$ GeV. Approximations of the total and differential cross-sections for such channels based on the model of Walker and Metcalf [30] were used up to 2 GeV. The excitation of six baryon resonances was taken into account. The contributions from $\Delta(1232)$, N$^\star(1520)$ and N$^\star(1680)$ are found

Table 5. Channels of the elementary γN interaction taken into account in the INC model.

γp-interaction	γn-interaction
$\gamma p \to \pi^+ n$	$\gamma n \to \pi^- p$
$\gamma p \to \pi^0 p$	$\gamma n \to \pi^0 n$
$\gamma p \to \pi^- \Delta^{++}$	$\gamma n \to \pi^- \Delta^+$
$\gamma p \to \pi^0 \Delta^+$	$\gamma n \to \pi^0 \Delta^0$
$\gamma p \to \pi^+ \Delta^0$	$\gamma n \to \pi^+ \Delta^-$
$\gamma p \to \eta p$	$\gamma n \to \eta n$
$\gamma p \to \omega p$	$\gamma n \to \omega n$
$\gamma p \to \rho^0 p$	$\gamma n \to \rho^0 n$
$\gamma p \to \rho^+ n$	$\gamma n \to \rho^- p$
$\gamma p \to \pi^+ \pi^- p$	$\gamma n \to \pi^+ \pi^- n$
$\gamma p \to \pi^0 \pi^+ n$	$\gamma n \to \pi^0 \pi^- p$
$\gamma p \to \pi^0 \pi^0 \pi^0 p$	$\gamma n \to \pi^0 \pi^0 \pi^0 n$
$\gamma p \to \pi^+ \pi^- \pi^0 p$	$\gamma n \to \pi^+ \pi^- \pi^0 n$
$\gamma p \to \pi^+ \pi^0 \pi^0 n$	$\gamma n \to \pi^- \pi^0 \pi^0 p$
$\gamma p \to \pi^+ \pi^+ \pi^- n$	$\gamma n \to \pi^+ \pi^- \pi^- p$
$\gamma p \to i\pi N (4 \le i \le 8)$ (35 channels)	$\gamma n \to i\pi N (4 \le i \le 8)$ (35 channels)

to be the most important. The presence of these resonances explains a well-known resonant structure in the total γN cross-section at $\omega \le 1.2$ GeV.

The channels $\gamma N \to 2\pi N$ and $\gamma N \to 3\pi N$ play a major role at $0.5 \le \omega \le 2$ GeV. These channels include also the resonant contributions from $\pi\Delta$, ηN, ρN and ωN channels (Table 5). Although the presence of these contributions in the total γN cross-sections is difficult to trace, the angular distributions of these channels have some specific features. Several examples may be given. The $\gamma p \to \eta p$ channel has three important contributions from $S_{11}(1535)$, $S_{11}(1700)$ and $P_{11}(1750)$ states. Due to the dominance of $S_{11}(1535)$, the angular distribution of the process is not far from isotropy. On the contrary, the $\gamma p \to \rho^0 p$ process has a prominent forward peak, since the non-resonant diffractive contribution dominates.

Many channels in the multi-pion reactions, $\gamma N \to i\pi N$, $(2 \le i \le 8)$, were not suitable for measurements in spark, bubble or streamer chamber experiments due to the presence of several neutral particles in the final state. However, one can reconstruct the integral cross-sections of undetectable channels by applying isotopic relations to the measured cross-sections of channels with charged particles, which can be found in compilation of ref. [27]. A phenomenological statistical approach for the exclusive description of the elementary γN interaction was applied to multiple pion production channels in ref. [18]. There the isospin symmetry was used to connect unknown cross-sections with measured ones. Other details of the method used for simulating the γN interaction may be found elsewhere, see ref. [18].

Since a huge number of multiple pion production channels is open at $\omega > 2$ GeV, the statistical description may be the only way to estimate the cross-sections of such channels. Recently another kind of statistical assumptions was used in the Monte Carlo event generator Sophia for simulating photohadronic processes in astrophysics [31].

2.4.2 Secondary processes

According to our model, the fast hadrons produced in a primary γN interaction initiate a cascade of successive quasi-free hadron-nucleon collisions inside the nucleus. The following elementary processes were taken into account:

$$\pi N \to \pi N,\ \pi(NN) \to NN,\ \pi N \to \pi\pi N;\ \pi N \to (i+1)\pi N,$$

$$NN \to NN,\ NN \to \pi NN,\ NN \to i\pi NN, (i \ge 2);$$

$$\eta N \to \eta N,\ \eta N \rightleftharpoons \pi N,\ \eta N \to \pi\pi N,$$

$$\eta(NN) \to NN,\ \eta(NN) \to \pi NN,$$

$$\omega N \to \omega N,\ \omega N \rightleftharpoons \pi N,\ \omega N \to \pi\pi N,$$

$$\omega(NN) \to NN,\ \omega(NN) \to \pi NN.$$

The empirical approximations for the measured total and differential cross-sections of the NN and πN interactions as well as the phenomenological estimations for the total and partial cross-sections of the ηN and ωN interactions were used in the calculation [18].

The described Monte Carlo model is implemented into the RELDIS code [11] which is especially designed for calculating the electromagnetic dissociation processes in ultrarelativistic heavy-ion collisions.

2.4.3 Characteristics of produced pions

The average number of pions, $\langle n_\pi \rangle$, produced in a γA process is quite small. The values of $\langle n_\pi \rangle$ for each pion charge are given in Table 6 for AuAu and PbPb collisions at RHIC and LHC energies, respectively. Even with the inclusion of multiple pion production channels ($\gamma N \to i\pi N$, $2 \le i \le 8$), the average numbers of pions of each charge are quite low (≈ 1). This can be explained by two reasons. First, in a great part of the electromagnetic dissociation events no real pions are produced at all, due to the dominance of soft photons ($\omega \le 140$ MeV) in the equivalent photon spectrum, eqs. (11),(14). Second, the most probable processes of pion production are $\gamma N \to \pi N$ and $\gamma N \to \pi\Delta$, which produce one or two pions only.

As one can see from Table 6, in the γA process the neutral pions are produced more abundantly as compared with π^+ and π^- mesons. A difference is noticeable also in the differential distributions, $d\sigma/dy$, shown in fig. 5 for each pion charge. The main deviations in the pion yields appear at rapidities close to the beam rapidity. This fact has a simple explanation. As already mentioned above,

Table 6. Average numbers of π^+,π^- and π^0 mesons produced in γA and grazing AA collisions.

	γA			AA		
	$\langle n_{\pi^+}\rangle$	$\langle n_{\pi^-}\rangle$	$\langle n_{\pi^0}\rangle$	$\langle n_{\pi^+}\rangle$	$\langle n_{\pi^-}\rangle$	$\langle n_{\pi^0}\rangle$
100A+100A GeV ^{197}Au on ^{197}Au	0.25	0.31	0.35	3.15	3.21	3.26
2.75A+2.75A TeV ^{208}Pb on ^{208}Pb	0.43	0.53	0.57	10.47	10.49	10.56

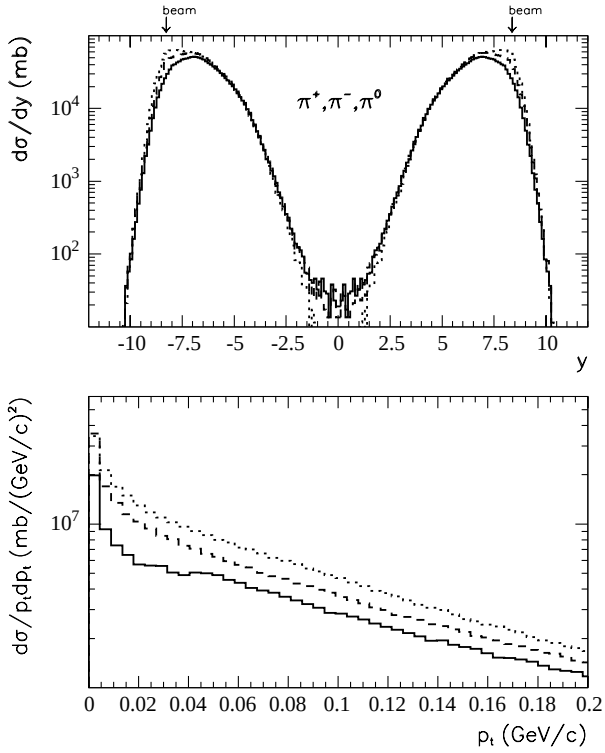

Fig. 5. Rapidity and transverse-momentum distributions of pions produced in γA process in PbPb collisions at LHC. The results of the RELDIS code are given by solid, dashed and dotted histograms for π^+, π^- and π^0 mesons, respectively. Beam rapidities are shown by arrows.

the process γN $\rightarrow$ πN dominates in the pion production by equivalent photons and the corresponding pions are close to the beam rapidity. This reaction can proceed on a proton: γp $\rightarrow$ π^+n, γp $\rightarrow$ π^0p and a neutron: γn $\rightarrow$ π^-p, γn $\rightarrow$ π^0n. Thus, single neutral pions can be produced both on the proton and the neutron, while π^+ on the neutron and π^- on the proton only. The total cross-sections of these four channels are close to each other. This gives the rate of the π^0 production approximately twice as large as the rate of π^+ or π^- or a light nucleus with equal numbers of protons and neutrons. This feature of the single-pion photoproduction is confirmed by the measurements of the inclusive cross-sections and the calculations made for carbon nucleus (see fig. 15 of ref. [18]).

Since a neutron excess exists in heavy nuclei like Pb or Au, in this case the π^- production will be enhanced in comparison with π^+, as is shown in fig. 5. The final-state interaction affects the absolute yields of the pions of different charges, but does not essentially change the ratio between them.

The detection of the pions produced close to the beam rapidity is a complicated experimental task. Special zero-degree detectors with proper identification of particle mass and charge are necessary for this purpose. However, if a forward detector located after a steering magnet is suitable for the determination of charges of nuclear fragments, one may exploit it to detect the pion emission process indirectly. If π^- is produced in the reaction γn $\rightarrow$ π^-p, it may be emitted while the recoil proton may be captured by the residual nucleus. The de-excitation of such nucleus may take place mainly via neutron emission. It means that the initial charge of the nucleus will be increased by one unit. The charge-to-mass ratio will be changed for such ion and it will be separated from the beam. Depending on the heavy-ion energy, the RELDIS code predicts the cross-section of such electromagnetic "charge pick-up" channels at the level of 10–100 mb. This process competes with the nucleon pick-up process via the strong interaction. Nevertheless, as is known from ref. [32], the cross-section of the latter process drops noticeably with increasing beam energy. On the contrary, the cross-section of the electromagnetic charge pick-up increases gradually with the beam energy and may essentially exceed the value of the cross-section for the nucleon pick-up due to the strong interaction.

The photonuclear reactions $(\gamma, \pi^- xn)$, $x = 0 - 9$, induced by bremsstrahlung photons were discovered many years ago. We refer the reader to a recent paper where such reactions were studied by radiochemical methods [33]. It would be interesting to study the same type of reactions induced by equivalent photons in ultrarelativistic heavy-ion collisions.

As mentioned above, the main part of pions is produced close to the beam rapidity. A small fraction of pions is produced by very high energy photons with $\omega \gg 10$ GeV. Some of the pions produced in such interactions may receive the momentum high enough to populate the central rapidity region. As shown in fig. 5, there are pions with $|y| < 5$ which may be confused with those from the $\gamma\gamma$ process. Therefore some selection criteria are necessary for detecting the $\gamma\gamma$ processes (see section 4).

3 Very peripheral nuclear collisions

Very peripheral (grazing) nuclear collisions with the participation of the strong nuclear forces can be misidentified as the electromagnetic interaction events. Both of these types of interactions contribute to the events with a low multiplicity of particles. To study the properties of strong interaction events the Monte Carlo event generator FRITIOF, version 7.1 [19] is used.

3.1 Basic elements of the FRITIOF model

Let us recall the main assumptions of the extended FRITIOF model [19] which is supposed to be valid up to the TeV energy region. FRITIOF is a Monte Carlo model for hadron-hadron, hadron-nucleus and nucleus-nucleus collisions. The basic idea of the model is in a simple picture that a struck hadron behaves like a relativistic string with a confined color field. This field is equivalent to that of a chain of dipoles lined up along the axis line. The dipole links act as partons. During the soft hadron-hadron interaction many small transverse momenta are exchanged between the dipole links and two longitudinally excited strings result from the collisions. A disturbance of the color field will in general initialise the gluonic radiation according to QCD. The final-state particles are produced by the string fragmentation like in the e^+e^- annihilation.

The large-p_t process can be treated by using QCD directly. The hard interaction effects, which are considered as the Rutherford parton scattering, become important in the TeV range of c.m. energies and at large $p_t > 1$ GeV/c. The results of the model are in good agreement with experimental hadron-hadron data up to the highest energies currently available.

Nucleus-nucleus collisions are regarded in the FRITIOF model as incoherent collisions between nucleons of colliding nuclei. FRITIOF does not take into account collective (coherence) effects when two nuclei interact as a whole. Thus a nucleon from the projectile interacts independently with the encountered target nucleons as it passes through the nucleus. Each of these subcollisions can be treated as a usual hadron-hadron collision. On the time scale of the collision process, the exited nucleon does not fragment inside the nucleus, so there are no intranuclear cascades. This assumption is reasonable at high energy since the time scale associated with fragmentation is much longer than the flight time of excited nucleons through the nucleus.

3.2 Nuclear density distributions and total cross-section in PbPb collisions

One of important aspects of the collision is the nuclear geometry. It is assumed that the projectile passes through the target nucleus on a straight line trajectory. The nucleons are distributed inside the nucleus according to the nuclear density distribution $\rho(r)$. In our calculations we use the Wood-Saxon density profile for heavy nuclei

$$\rho(r) = \frac{\rho_0}{1 + \exp(\frac{r - r_0 A^{1/3}}{C})}, \qquad (15)$$

where $r_0 = 1.16(1 - 1.16A^{-2/3})$ is the radial scale parameter, C is the diffuseness parameter which is slightly A-dependent (its values used in the program ranging from 0.47 to 0.55 fm) and ρ_0 is a normalisation constant. Then for lead nucleus the radius defined at the half of the normal nuclear density is equal to $R = r_0 A^{1/3} = 6.63$ fm, while the diffuseness parameter used by FRITIOF is equal to $C = 0.545$ fm.

The total cross-section of the strong lead-lead interaction at LHC collider was estimated to be 7164 mb, according to a simple geometrical formula used in ref. [34]. This estimation does not take into account the energy dependence of the total nucleus-nucleus cross-section due to the increase of the total nucleon-nucleon cross-section. By using the extrapolations of the measured pp cross-sections to LHC energies one can obtain a higher value of about 10 barn, see ref. [35]. For this value of the total nucleus-nucleus cross-section one has to rescale the plots given in the present paper by 30% for grazing nuclear collisions.

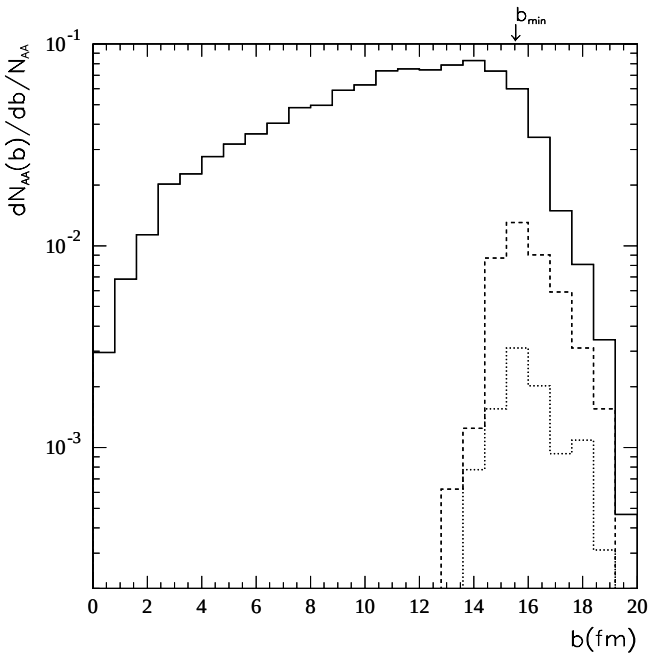

Fig. 6. Impact parameter distributions for nuclear PbPb collisions at LHC simulated by the FRITIOF code. The solid histogram corresponds to all events. The dotted and dashed histograms present the impact parameter distributions for events with $N_{\pi^0} = 1$ and $N_{\pi^0} = 2$, respectively.

3.3 Impact parameter distribution in nuclear collisions

Special efforts should be undertaken to find proper ranges of the impact parameter b which divide nucleus-nucleus

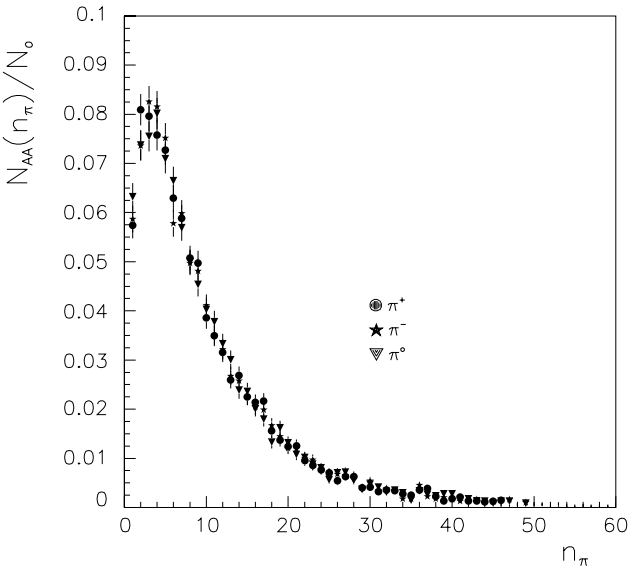

Fig. 7. Pion multiplicity distributions for grazing nuclear PbPb collisions at LHC simulated by the FRITIOF code. The events with impact parameter $b \geq 15.5$ fm were selected.

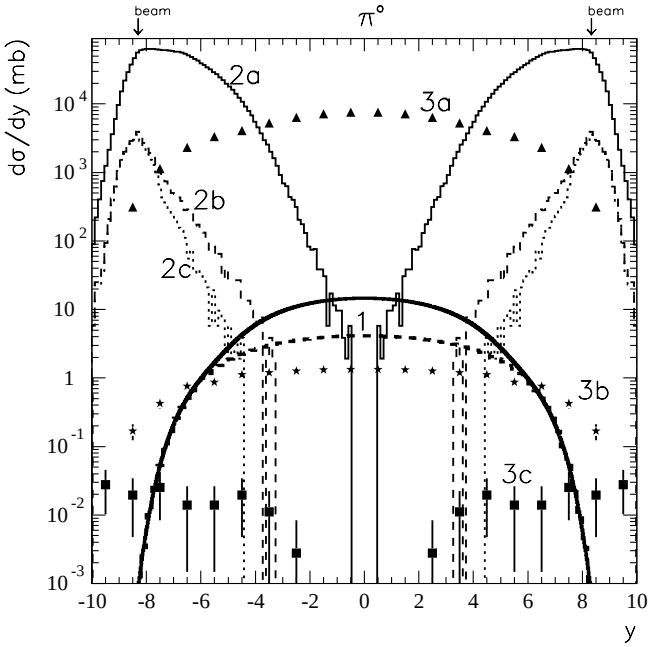

Fig. 8. Rapidity distribution of π^0 produced in peripheral PbPb collisions at LHC energies. The thick solid and dashed line histograms labeled "1" are the inclusive (the DRP model) and exclusive cross-sections for π^0 production in $\gamma\gamma$ fusion. The histograms "2a","2b" and "2c" give the results of the RELDIS code for γA process. The FRITIOF results for peripheral PbPb collisions with $b \geq 15.5$ fm are given by the symbols labeled "3a","3b" and "3c". The distributions with label "a" were obtained without p_t cuts. The label "b" corresponds to the selection of events with the total transverse momentum of meson system $|\mathbf{p}_t{}^{(\mathrm{sum})}| \leq 75$ MeV/c. The label "c" corresponds to the selection of events with $|\mathbf{p}_t| \leq 75$ MeV/c for each of the pions including π^0, π^+, and π^-.

collisions into different categories. As explained in the introduction, most important for us are very peripheral nuclear collisions and electromagnetic interactions, further subdivided into the $\gamma\gamma$ and γA events.

The uncertainties associated with the diffuseness of the nuclear density distribution affect greatly the resulting ranges. We used the FRITIOF model to define these ranges. The impact parameter distribution of events simulated by the FRITIOF code is given in fig. 6. The plotted quantity $\mathrm{d}N_{\mathrm{AA}}(b)/\mathrm{d}b/N_{\mathrm{AA}}$ is a relative number of nuclear collisions with a given b. As is shown in the figure, the events with a low multiplicity of pions correspond to the collisions with $12 \leq b \leq 20$ fm. It is the domain of b which defines the grazing nuclear collisions with the participation of the strong nuclear forces. It should be stressed however, that this definition is essentially model dependent and numerical results may be different if one uses another code with a different treatment of the diffuse boundary of the nucleus and another value of the elementary NN cross-section.

We see that the value which defines the onset of electromagnetic collision for PbPb ions, $b_{\min} = 15.5$ fm, used in the paper [10] does not contradict the results of the FRITIOF calculations given in fig. 6. Following our previous papers [10,11], for consistency we define the end of the nuclear overlap in lead-lead collisions at $b_{\min} = 15.5$ fm. This choice is also supported by the calculation of ref. [36] where the average number of interacting nucleons, $\langle N_{\mathrm{in}} \rangle$, was evaluated as a function of b for the case of PbPb collisions. As it was found [36], $\langle N_{\mathrm{in}} \rangle \approx 1$ at $b = 15.5$ fm. According to the Wood Saxon density function for Pb nucleus, it corresponds to the overlap of those boundary regions of the colliding nuclei which have the nuclear densities below 0.1 of the value at the center of the nucleus. The total number of such events in the FRITIOF simulation turns out to be 24%.

Figure 7 demonstrates the distribution of pion multiplicities for peripheral PbPb collisions ($b \geq 15.5$ fm) at LHC energies simulated by the FRITIOF code. The most probable is the production of four pions and the distribution is very broad. This conclusion is valid for all the charge states of pions. The average pion multiplicities are given in Table 6, where one can see that the multiplicities of the pions produced in the above-defined grazing AA collisions are generally greater than those for the γA process.

4 Comparison of different mechanisms of pion production

Since most of the detectors used thus far in heavy-ion experiments have very restricted acceptance on rapidity, it is important to investigate the rapidity dependence of the pion production cross-section. Rapidity distributions of neutral pions produced in peripheral PbPb collisions at LHC energies are shown in fig. 8.

Let us consider first the distributions without any additional selection criteria. The distributions from the $\gamma\gamma$

fusion and grazing nuclear collisions calculated by the FRITIOF code with $b \geq 15.5$ fm are very similar in shape. The distributions of $\mathrm{d}\sigma/\mathrm{d}y$ for the single and inclusive π^0 production in the $\gamma\gamma$ fusion also have maximuma at $y = 0$. But even in this region it is much lower than the contribution from grazing nuclear collisions. On the contrary, the rapidity distribution for the γA process peaks at the beam and target rapidities. Nevertheless, its contribution at the midrapidity is comparable to one from the $\gamma\gamma$ fusion.

The above-described picture is unfavourable for experimental detection of the pions from $\gamma\gamma$ collisions. Nonetheless, one can improve the detection conditions by introducing appropriate transverse momentum cuts. Indeed a single meson from the $\gamma\gamma$ fusion has a very small transverse momentum. Selecting events with low values of p_t one can reject contributions from other processes. Following this way, two different p_t–cut procedures may be proposed.

According to the first procedure (b-criterion), one should select the events with a small total transverse momentum of the meson system $|\mathbf{p}_\mathrm{t}^{(\mathrm{sum})}| \leq 75$ MeV/c. The second selection procedure (c-criterion) imposes more severe restrictions on the transverse momenta of the produced pions demanding each of them (including π^0, π^+, and π^-) to be small, $|\mathbf{p}_\mathrm{t}| \leq 75$ MeV/c, in this case. As one can see, the b-criterion is equivalent to the c-criterion in the case of the single-pion production.

Let us investigate now to what extent the rapidity distributions are affected by the p_t cuts. The distributions obtained according to the b- and c-criteria are also given in fig. 8. One can see that the b-criterion reduces the contribution from grazing nuclear collisions by three orders of magnitude and gives some benefits for the detection of $\gamma\gamma$ events. If this reduction is not sufficient, one can use the c-criterion which is more efficient. Further suppression of the pions from grazing nuclear collisions may be obtained in the region $-4 < y < 4$. With this suppression even the exclusive $\gamma\gamma \to \pi^0$ channel may be clearly distinguished.

The difference in the b- and c-criteria applied to the γA events calculated by the RELDIS code is less prominent. This is explained by the fact that the single-pion production dominates in the γA collisions at $\omega \geq 140$ MeV while the b- and c-criteria are equivalent for this case. Both of the procedures may be recommended to reduce the contribution from the γA process as it is shown in fig. 8.

It should be noticed that the b-criterion does not affect the inclusive distribution for the $\gamma\gamma$ fusion, while the c-criterion suppresses the main part of the events of π^0 production due to heavy-meson decays. This may be useful for mesuring the exclusive $\gamma\gamma \to \pi^0$ process.

5 Conclusions

Only several hadrons are produced on average in very peripheral collisions of ultrarelativistic heavy ions. Because of this feature such collisions can be considered as non-violent events. The exact determination of the impact parameter in a collision event is beyond present experimental techniques. However, as is shown in the present paper, selecting the events with low multiplicity of produced mesons, one can approximately identify a domain of large impact parameters where the $\gamma\gamma$ fusion, γA or grazing nuclear AA collisions takes place.

Calculations show that each of the mechanisms has a specific distribution of the produced pions on the transverse momentum, p_t, and rapidity, y. One can use these features for adjusting detectors to different regions of p_t and y with the possibility to disentangle pions produced by different mechanisms. One can enhance the signal-to-background ratio for the $\gamma\gamma$ fusion by selecting events with a low p_t by means of two procedures considered in the paper. Our preliminary results confirm the importance of the p_t cut proposed in ref. [12]. This procedure rejects the background from γA and grazing AA collisions by several orders of magnitude. Moreover, using p_t cuts one can avoid a pessimistic conclusion made in ref. [37] that the $\gamma\gamma$ fusion is indistinguishable from other processes since the rapidity distributions for these processes are very similar to each other.

LIS and APK are grateful to Dr. Kai Hencken for useful discussions and a possibility to use his code for comparison. IAP is indebted to INTAS for the financial support from Young Scientists Fellowship 98-86 and thanks the Niels Bohr Institute for the warm hospitality. The work is supported in part by the Universities of Russia Basic Research Fund, grant 5347, RFBR-DFG grant 99-02-04011 and by the Humboldt Foundation, Germany.

References

1. *The Large Hadron Collider Accelerator Project*, CERN/AC/93-03(LHC), 1993.
2. *Conceptual design of the relativistic heavy ion collider RHIC*, BNL 52195 UC-414, 1989.
3. M. Asakawa, H. Minakata and B. Müller, Nucl. Phys. A **638**, 433c (1998).
4. P.F. Kolb, J. Sollfrank, U. Heinz, Phys. Lett. B **459**, 667 (1999).
5. H. Heiselberg and A.-M. Levy, Phys. Rev. C **59**, 2716 (1999).
6. C.A. Bertulani and G. Baur, Phys. Rep. **163**, 299 (1988).
7. F. Krauss, M. Greiner and G. Soff, Prog. Part. Nucl. Phys. **39**, 503 (1997).
8. G. Baur, K. Hencken, D. Trautmann, J. Phys. G **24**, 1657 (1998).
9. S. Datz, J.R. Beene, P. Grafström, H. Knudsen. H.F. Krause, R.H. Schuch and C.R. Vane, Phys. Rev. Lett. **79**, 3355 (1997).
10. I.A. Pshenichnov, I.N. Mishustin, J.P. Bondorf, A.S. Botvina, A.S. Iljinov, Phys. Rev. C **57**, 1920 (1998).
11. I.A. Pshenichnov, I.N. Mishustin, J.P. Bondorf, A.S. Botvina, A.S. Iljinov, Phys. Rev. C **60**, 044901 (1999).
12. G. Baur, K. Hencken, D. Trautmann, S. Sadovsky and Yu. Kharlov, CMS NOTE 1998/009.
13. M. Grabiak, B. Müller, W. Greiner, G. Soff, P. Koch, J. Phys. G **15**, L25 (1989).
14. S. Klein and J. Nystrand, STAR Note 347, 1998.
15. J. Nystrand, S. Klein and STAR Collaboration, LBNL-42524, nucl-ex/9811007.

16. *CMS Technical proposal*, CERN/LHCC-94-38, LHCC/P1, 1994.
17. S. Klein and J. Nystrand, Phys. Rev. C **60**, 014903 (1999).
18. A.S. Iljinov, I.A. Pshenichnov, N. Bianchi, E.De Sanctis, V. Muccifora, M. Mirazita and P. Rossi, Nucl. Phys. A **616**, 575 (1997).
19. B. Andersson, G. Gustafson, Hong Pi, Z. Phys. C **57**, 485 (1993).
20. G. Baur and L. Fereira Filho, Nucl. Phys. A **518**, 786 (1990).
21. C. Caso et al. (Particle Data Group), *Review of Particle Physics*, Eur. Phys. J. C **3**, 1 (1998).
22. M. Vidovic, M. Greiner, C. Best, G. Soff, Phys. Rev. C **47**, 2308 (1993).
23. C.A. Bertulani and G. Baur, Nucl. Phys. A **458**, 725 (1986).
24. G. Singh, P.L. Jain, Z. Phys. A **344**, (1992) 73.
25. W.J. Llope and P. Braun-Munzinger, Phys. Rev. C **41**, 2644 (1990).
26. K. Ukai and T. Nakamura, *Data Compilation of Single Pion Photoproduction below 2 GeV*, INS-T-550(1997).
27. HERA and COMPAS Groups, S.I. Alekhin *et al.* , *Compilation of cross-sections: IV γ, ν, Λ, Σ, Ξ and K_L^0 induced reactions*, CERN-HERA 87-01, Geneva, 1987.
28. V.S. Barashenkov, F.G. Gereghi, A.S. Iljinov, G.G. Jonsson and V.D. Toneev, Nucl. Phys. A **231**, 462 (1974).
29. P. Corvisiero, L. Mazzaschi, M. Ripani, M. Anghinolfi, V.I. Mokeev, G. Ricco, M. Taiuti, A. Zucchiatti , Nucl. Instrum. Meth. A **346**, 433 (1994).
30. R.L. Walker, Phys. Rev. **182**,(1969) 1729; W.J. Metcalf, R.L. Walker, Nucl. Phys. B **76**, 253 (1974).
31. A. Mucke, R. Engel, J.P. Rachen, P.J. Protheroe, T. Stanev, Comp. Phys. Commun. **124**, 290 (2000).
32. B.S. Nilsen, C.J. Waddington, W.R. Binns, J.R. Cummings, T.L. Garrand, L.Y. Geer and J. Klarmann, Phys. Rev. C **50**, 1065 (1994).
33. K. Sakamoto, S.R. Sarkar, Y. Oura, H. Haba, H. Matsumura, Y. Miyamoto, S. Shibata, M. Furukawa, I. Fujiwara, Phys. Rev. C **59**, 1497 (1999).
34. Y.D. He, P.B. Price, Z. Phys. A **348**, (1994) 105.
35. V.L. Korotkikh and I.P. Lokhtin, Phys. At. Nucl. (Yad. Fiz.) **56**, (1993) No. 8, 1110.
36. C. Pajares and Yu.M. Shabelski, hep-ph/9811214.
37. R. Engel, M.A. Braun, C. Pajares and J. Ranft, Z. Phys. C **74**, 687 (1997).